

SCIENTIFIC REPORTS

OPEN

Luminescent manganese-doped CsPbCl₃ perovskite quantum dots

Chun Che Lin¹, Kun Yuan Xu¹, Da Wang² & Andries Meijerink¹

Received: 21 November 2016

Accepted: 01 February 2017

Published: 12 April 2017

Nanocrystalline cesium lead halide perovskites (CsPbX₃, X = Cl, Br, and I) form an exciting new class of semiconductor materials showing quantum confinement. The emission color can be tuned over the full visible spectral region making them promising for light-emitting applications. Further control over the optical and magnetic properties of quantum dots (QDs) can be achieved through doping of transition metal (TM) ions such as Mn²⁺ or Co²⁺. Here we demonstrate how, following QD synthesis in the presence of a Mn-precursor, dropwise addition of silicon tetrachloride (SiCl₄) to the QDs in toluene results in the formation of Mn-doped CsPbCl₃ QDs showing bright orange Mn²⁺ emission around 600 nm. Evidence for successful doping is provided by excitation spectra of the Mn²⁺ emission, with all features of the CsPbCl₃ QD absorption spectrum and a decrease of the 410 nm excitonic emission life time with increasing Mn-concentration, giving evidence for enhanced exciton to Mn²⁺ energy transfer. As a doping mechanism we propose a combination of surface etching and reconstruction and diffusion doping. The presently reported approach provides a promising avenue for doping TM ions into perovskites QDs enabling a wider control over optical and magnetic properties for this new class of QDs.

Lead halide perovskites MPbX₃ (where M = CH₃NH₃⁺, HC(NH₂)₂⁺, and Cs⁺; X = Cl, Br, and I) have recently gained interest as the result of their promising performance for a variety of optoelectronic applications, especially photovoltaics^{1–3}, but also light-emitting diodes (LEDs)^{4,5}, lasing^{6,7}, and photodetectors^{8,9}. These materials have favorable intrinsic properties including broad absorption spectra, tunable optical spectra, high luminescence quantum yields, high carrier mobility, and long carrier diffusion length. In the past three years, a rapidly increasing number of studies were published focused on synthetic methods and morphology control of colloidal perovskites nanocrystals (NCs) aimed at improving their performance in practical applications. The hybrid organic–inorganic perovskites materials, such as CH₃NH₃PbX₃ (X = Cl, Br, and I), are outstanding solar harvesting materials in photovoltaic devices with 20% certified power conversion efficiencies^{10,11}. Sargent *et al.* utilized perovskites shell-capped colloidal QDs films of (PbS–CH₃NH₃PbI₃) to fabricate novel and efficient photovoltaic devices¹².

The all inorganic analogue perovskites CsPbX₃ QDs were soon after reported by Kovalenko *et al.*¹³. These QDs show efficient luminescence that can be tuned over the full visible spectrum (400–700 nm) by tuning of size (through quantum confinement effects) and composition (anion exchange)^{13,14}. Using a facile solution-based synthesis approach, cubic CsPbX₃ QDs with colorful narrow emission bands and high quantum yields of up to 90% were realized¹³. The highly efficient narrow band emission makes these QDs very useful for application in lighting and displays. For example, colloidal CsPbBr₃ QDs have been reported with efficient narrow band emission (FWHM = 86 meV; quantum yield = 90%) and reduced emission blinking making them promising for the lighting and display industry¹⁵. Interestingly, it is not generally known that this class of CsPbX₃ QDs has been known for almost 20 years. Emission and quantum confinement of CsPbX₃ QDs that form in Pb-doped CsX scintillator crystals was reported in the late 1990s¹⁶. For the II–VI QDs such as ZnO, ZnS, ZnSe, CdS, CdSe there has been a strong effort to dope the QDs with transition metal (TM) ions such as Mn²⁺ or Co²⁺ aimed at introducing new optical and/or magnetic functionalities^{17–21}. A large number of publications have reported different categories of doped QDs^{22–24}. For example, efficient Mn²⁺ emission in ZnSe QDs is promising for application in solar concentrators as a result of the large spectral shift of the Mn²⁺ emission which prevents undesired reabsorption²⁵. Doping of magnetic ions in QDs also holds great promise in the field of spintronics with the possibility to dope a single magnetic ion in a single QD.

¹Condensed Matter and Interfaces, Debye Institute for Nanomaterials Science, Utrecht University, Princetonplein 5, 3584 CC Utrecht, The Netherlands. ²Soft Condensed Matter, Debye Institute for Nanomaterials Science, Utrecht University, Princetonplein 5, 3584 CC Utrecht, The Netherlands. Correspondence and requests for materials should be addressed to A.M. (email: a.meijerink@uu.nl)

Doping can be straightforward by simply adding a dopant precursor in the reaction mixture, e.g. in ZnS:Mn²⁺, but more often doping of QDs proved to be challenging²⁶. In the past decade new doping techniques have been developed allowing doping of systems that were previously considered not possible to dope. For example, doping CdSe with Mn²⁺ was considered impossible but was later realized using a single source precursor method. More recently with diffusion doping even concentrations up to 30% Mn²⁺ are now incorporated in CdSe²⁷. For perovskite QDs doping has only recently been realized and is highly interesting as it allows the addition of optical or magnetic functionalities to this exciting new class of materials^{28,29}.

Here we report doping of Mn²⁺ into perovskite CsPbCl₃ QDs (CPC–Mn) via a facile colloidal approach. A post synthesis treatment of CsPbCl₃ QDs prepared in the presence of Mn–stearate allows incorporation of Mn²⁺. Slowly dripping a small volume (5–20 μl) of SiCl₄ to the dispersion of QDs in toluene results in a slow incorporation of Mn²⁺ at room temperature. Evidence for successful doping is provided by a clear signature of efficient energy transfer from the CsPbCl₃ QD exciton to Mn²⁺ ions. As Mn²⁺ incorporation proceeds, the excitonic emission intensity decreases and the bright orange Mn²⁺ emission increases. The excitation spectrum of the Mn²⁺ emission shows all the features of the CsPbCl₃ QD exciton absorption. The life time of the exciton emission decreases as the Mn²⁺ concentration increases as a result of fast exciton to Mn²⁺ energy transfer. The proposed mechanism for incorporation involves surface etching and reconstruction and diffusion doping. Decomposition of SiCl₄ by trace amounts of water in the toluene yields HCl. Surface etching by H⁺ and surface reconstruction enabled by chloride ions and Mn²⁺ form a surface layer and slowly drives Mn²⁺ into the QDs by ion diffusion. The decomposition of SiCl₄ also gives rise to the formation of a protective SiO₂ layer giving a relatively high stability to the QDs. Perovskites QDs are known to degrade and show a fast loss of emission intensity under ambient conditions. The PL of the CPC–Mn QDs synthesized is relatively stable and retains over 25–30% of the maximum intensity after stirring with SiCl₄ for 40 days.

Results and Discussion

Synthesis and characterization. CsPbCl₃ QDs were prepared using a similar procedure as reported by Kovalenko *et al.*¹³. Details on the QD synthesis and doping procedure can be found in the Methods section. In short, PbCl₂ and the Mn–precursor (Mn–stearate) in 1–octadecene (ODE) were dried at 120 °C after which dried oleylamine (OLAM) and oleic acid (OA) were added. The temperature was raised to 170 °C and a Cs–oleate solution in ODE was injected. At this temperature the CsPbCl₃ QDs form quickly. Next, the mixture was cooled and the NCs were extracted by centrifugation. To remove unreacted polar material the QD precipitate was redispersed in toluene and centrifuged. Precipitated particles were discarded. The final solution of CsPbCl₃ QDs in toluene shows the characteristic violet QD emission but no Mn²⁺ emission, indicating that in this procedure Mn²⁺ is not incorporated. In the next step a small volume (5–20 μl) of SiCl₄ was dripped to 2 ml of the QD solution. During stirring a white precipitate forms. After different stirring times the precipitate was removed by centrifugation and a transparent QD solution was used for the spectroscopic measurements and characterization. As a control experiment SiCl₄ was also added under vacuum conditions in which all water was removed from the toluene.

In Fig. 1a X–ray diffraction (XRD) patterns of the various synthesis products are shown. Line 1 (blue) shows the typical XRD pattern of CsPbCl₃ QDs made without Mn²⁺. The XRD pattern of the QDs synthesized in the presence of the Mn–stearate precursor (green line) is similar. For the product formed after addition of SiCl₄ and stirring for 1 h (red line) the formation of amorphous SiO₂ is evident from the broad diffraction peak of amorphous SiO₂ (PDF Card No. 82–1576), observed clearly from 15° to 30°. Stirring for 10 days, the pure CsPbCl₃ XRD patterns (black line) was still found when the precipitate (SiO₂) was removed by centrifuging. The lines in the XRD patterns of the QDs match the powder diffraction pattern of cubic phase CsPbCl₃ (Fig. S1a). The broadening of the diffraction peaks is because of the small size. The TEM image (Fig. 1b) shows the formation of monodisperse (13.1 ± 0.4 nm) side length CPC–Mn QDs and a d–spacing of 0.58 nm is clearly observed^{13,30}. The particle size is similar to that for samples made without Mn–precursor (Fig. S2). Figure S3 displays elemental analysis by energy dispersive X–ray spectroscopy (EDX) to confirm that Mn is present in the sample after doping, although no Mn²⁺ emission is observed. Given the highly apolar nature of the Mn–precursor, the Mn–stearate can be expected to absorb in the apolar capping layer around the QDs.

In the next step a small volume of SiCl₄ is added to the QDs in toluene. The role of this silica precursor is twofold: it will induce the growth of protective SiO₂ around the QD, and, more importantly, it induces the incorporation of Mn²⁺ in the CsPbCl₃ QDs. The role of SiO₂ as a protective shell to protect the core material is well-known. For example, the stability of CH₃NH₃PbBr₃–SiO₂³¹, CdSe/ZnS–SiO₂³², and CdSe/CdS/ZnS–SiO₂³³, QDs were clearly improved in comparison to the uncoated QDs. The High Angle Annular Dark Field Scanning TEM (HAADF–STEM) image after addition of SiCl₄ and stirring for 10 days and removal of SiO₂ by centrifugation is shown in Fig. 1c. The monodisperse cubic particles (7.7 ± 0.5 nm) are smaller than that for the QDs before SiCl₄ addition. This indicates that SiCl₄ addition causes etching of the CsPbCl₃ QDs. In the HAADF–STEM images also white dots are observed. Elemental mapping (Fig. S4) reveals that these dots are highly enriched in Pb.

In the HAADF–STEM image of the sample before centrifugation both individual CPC–Mn QDs and SiO₂ nanoparticles were observed (Fig. 1d). This indicates that also a secondary nucleation of silica occurred and that silica was not only deposited on the QD surface in a seeded growth. EDX analysis for a region containing CPC–Mn QDs (cyan square Fig. 1d) and a region containing mainly SiO₂ (cyan circle Fig. 1d) are shown in Fig. 1e and f. In the EDX spectrum of the QD area (cyan square) signals of Cs, Pb, Cl, and Mn of the CPC–Mn QDs are observed and signals corresponding to Si and O are weak. The elemental analysis of the cyan circle shows strong Si and O signals, indicating the presence of a SiO₂ nanoparticles.

In a control experiment, SiCl₄ was added to the QD dispersion and then stirred for 3 days in vacuum. TEM image and EDX analysis were recorded for the CPC–Mn QDs made under vacuum are shown in Fig. S5. The CPC–Mn QDs were covered by a SiO₂ layer (Fig. S5a). The different SiO₂ morphology is ascribed to a difference in water content which determines the HCl concentration following hydrolysis of SiCl₄^{34,35}. The water present in

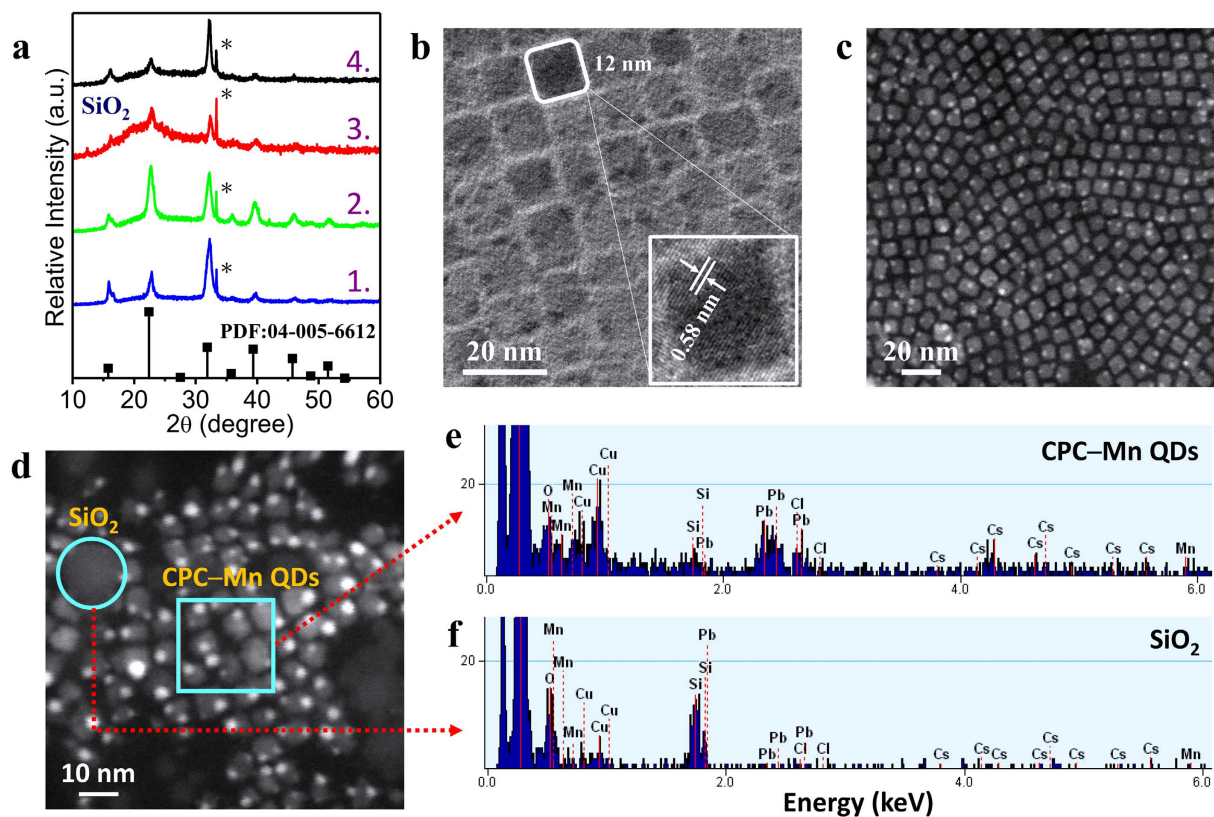


Figure 1. Characterization of CPC-Mn QDs. (a) X-ray diffractograms of as synthesized CsPbCl_3 (1), CsPbCl_3 with added Mn^{2+} -precursor (2), CsPbCl_3 with Mn^{2+} -precursor after addition of SiCl_4 and stirring for 1 h (3) and 10 days (4) compared to the standard powder diffraction pattern (black vertical lines) of cubic bulk CsPbCl_3 (* marks extra peaks are caused by the silicon wafer). (b) TEM image of the CPC-Mn QDs. The inset shows a higher magnification image of a cubic particle. (c) HAADF-STEM image of the CPC-Mn QDs (after centrifuging) with SiCl_4 and stirring 10 days. (d) HAADF-STEM image of the CPC-Mn QDs (solution without centrifuging) with SiCl_4 for stirring 10 days. (e, f) EDX analysis for a CPC-Mn QDs region (cyan square) and a region without QDs (cyan circle) from Fig. 1d.

toluene under ambient conditions (H_2O content $\sim 0.06\%$) induces faster decomposition of SiCl_4 and silica formation³¹. In the resulting SiO_2 covered CPC QD conglomerates all elemental signals of the CPC-Mn QDs and SiO_2 (Cs, Pb, Cl, Mn, Si, and O) were observed, as shown in Fig. S5b.

Optical spectroscopy. To monitor incorporation of luminescent dopants into QDs optical and time resolved spectroscopy are powerful tools. When a luminescent ion is inside of a QD, fast energy transfer from the QD exciton to the dopant is expected. Absorption of light by the QD is followed by exciton-to-dopant energy transfer and emission from the dopant ion. Monitoring emission and excitation spectra as well as changes in the time traces of the luminescence intensity of excitonic and dopant emission provides clear signatures for the successful incorporation of a dopant in a QD. In Fig. 2a,b absorption, excitation, and emission spectra are shown for three types of CsPbCl_3 QDs: undoped QDs (CPC, no Mn added, green lines), CsPbCl_3 :5%Mn QDs (CPC:5%Mn, 5% Mn-precursor added to reaction mixture, red lines) and CsPbCl_3 :5%Mn- SiCl_4 (CPC:5%Mn- SiCl_4 , 5% Mn-precursor added, followed by 10 μl SiCl_4 and stirring for 1 day, blue lines). All three QDs show exciton emission around 400–410 nm. The emission spectra of the CPC and CPC:5%Mn samples are almost identical. For the CPC:5%Mn- SiCl_4 sample an extra emission band is observed in the red/orange spectral region around 600 nm. The excitonic emission shows a small (5 nm) blue shift and is slightly broader (halfwidth = 600 cm^{-1} versus 550 cm^{-1} for the CPC and CPC:5%Mn- SiCl_4 exciton emission).

The 600 nm emission wavelength is typical of the ${}^4\text{T}_1 \rightarrow {}^6\text{A}_1$ emission from Mn^{2+} . Mn^{2+} can emit in the green to deep red spectral region depending on the local coordination. The Tanabe-Sugano diagram for ions with the $3d^5$ configuration shows that the position of the emitting lowest energy excited state ${}^4\text{T}_1$ shifts to lower energies as the crystal field splitting increases^{36,37}. In CsPbCl_3 the Mn^{2+} will substitute on the octahedrally coordinated Pb^{2+} site (the Cs^+ -site is too large). Since Cl^- ions are weak crystal field ligands in the spectrochemical series a green emission may be expected. However, octahedral coordination gives rise to a large crystal field splitting and even for weak ligands orange-red emission is typically observed for Mn^{2+} . For example, in CdCl_2 and a variety of chloride perovskites where Mn^{2+} is in an octahedral Cl^- coordination, the emission maximum of the ${}^4\text{T}_1 \rightarrow {}^6\text{A}_1$ emission of Mn^{2+} has been observed at wavelengths varying between 570 nm and 630 nm^{36,37}. The presently

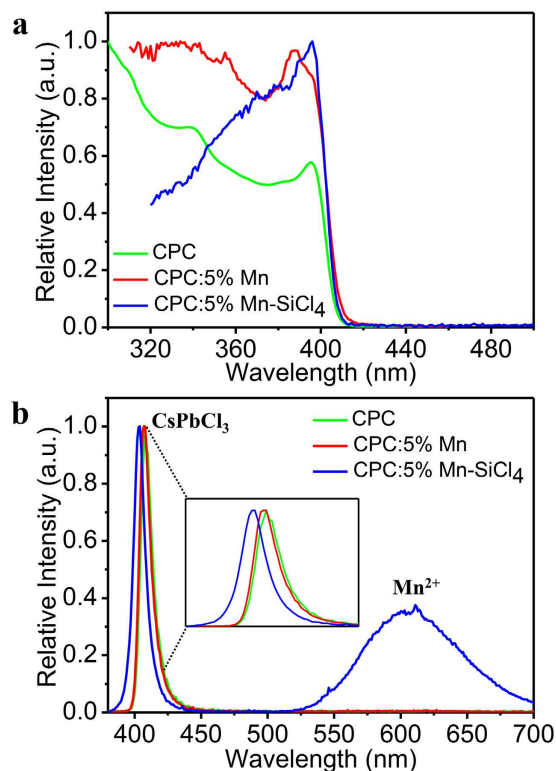


Figure 2. Optical properties of the CsPbCl₃:5%Mn²⁺ QDs. (a) Absorption spectrum (green line) of undoped CsPbCl₃ NCs. Excitation spectra of the CsPbCl₃:5%Mn²⁺ (red line) and CsPbCl₃:5%Mn²⁺ after SiCl₄ addition and stirring for 1 day (blue line). (b) Emission spectra of the undoped CsPbCl₃ (green), CsPbCl₃:5%Mn²⁺ (red) and CsPbCl₃:5%Mn²⁺ QDs after SiCl₄ addition and 1 day stirring (blue).

observed emission maximum at 600 nm is in excellent agreement with this range and provides further support for the assignment of the orange emission to ⁴T₁–⁶A₁ emission of Mn²⁺ in an octahedral Cl⁻ coordination.

The absorption and excitation spectra of the different CPC QDs in Fig. 2a are all similar and show an exciton peak at 410 nm. Interestingly, the excitation spectrum of the red/orange Mn²⁺ emission for the CPC:5%Mn–SiCl₄ QDs (blue line) also shows the excitonic features of the QD absorption, indicating exciton-to-Mn²⁺ energy transfer, a signature of incorporation of Mn²⁺ in the CsPbCl₃ QD. Careful inspection of the emission spectra for CPC:5%Mn before SiCl₄ addition reveals a very weak emission feature in the orange spectral region (Fig. S6) that is not observed for the undoped CPC sample (Fig. 2b, green line). The weak Mn²⁺ emission disappears after washing with acetone (see Fig. S7) and also no Mn²⁺ emission was observed for acetone-washed CPC:5%Mn after addition of SiCl₄ under ambient conditions. This result indicates that the weak emission originates from Mn²⁺ precursor adsorbed in the QD surface layer. As the Mn²⁺ ions are not incorporated in the QD, energy transfer from the exciton to Mn²⁺ excited states is not efficient due to the weak coupling of the exciton to remote Mn²⁺ ions. Washing with acetone removes the surface adsorbed Mn²⁺ precursor.

As shown above, the addition of a small volume of SiCl₄ to the CPC QDs in toluene gives rise to Mn²⁺ emission after prolonged stirring at room temperature. To study the influence of the volume of SiCl₄ added, emission spectra were recorded after addition of 5–20 μl SiCl₄ into the CPC:5%Mn QDs toluene solution under ambient conditions. The emission spectra, shown in Fig. S8, show an enhanced CPC exciton emission as well as Mn²⁺ emission for all solutions after 12 h of stirring following SiCl₄ addition. The increase in PL intensity is explained by better surface passivation of the QDs and will be discussed below. The intensity of the Mn²⁺ emission increases for SiCl₄ volumes up to 10 μl and then decreases. For the highest volumes added (15 or 20 μl SiCl₄) degradation of the CsPbCl₃ QDs was observed. As the stability of the CPC QDs is compromised, also the Mn²⁺ emission intensity decreased for the highest volumes of SiCl₄ added. For the reaction volume used (2 ml), the optimum SiCl₄ amount equals 10 μl and this volume was used in subsequent experiments to follow the time evolution of Mn²⁺ incorporation.

To optimize the Mn-concentration and to probe Mn-incorporation over time, extensive spectroscopic characterization was done for CPC:x%Mn–SiCl₄ samples taken at different times after injection of SiCl₄. In Fig. 3 excitation and emission spectra, luminescence decay curves of the excitonic and Mn²⁺ emission as well as the integrated emission intensity ratios of Mn/QD are shown for different times (1 hour to 10 days) after injection of 10 μl SiCl₄ to a CPC:x%Mn QD dispersion prepared with 1, 3, 5, 7 and 10% of Mn-precursor present in the initial reaction (concentrations in mole% relative to Pb²⁺). Figure 3a shows the ratio of the Mn²⁺ to QD emission intensity for samples taken after 1 h to 10 days. In Fig. 3b,c photographs are shown of the QD dispersions under UV (365 nm) illumination after 1 h and 10 days of stirring. In the photographs a clear change in emission color

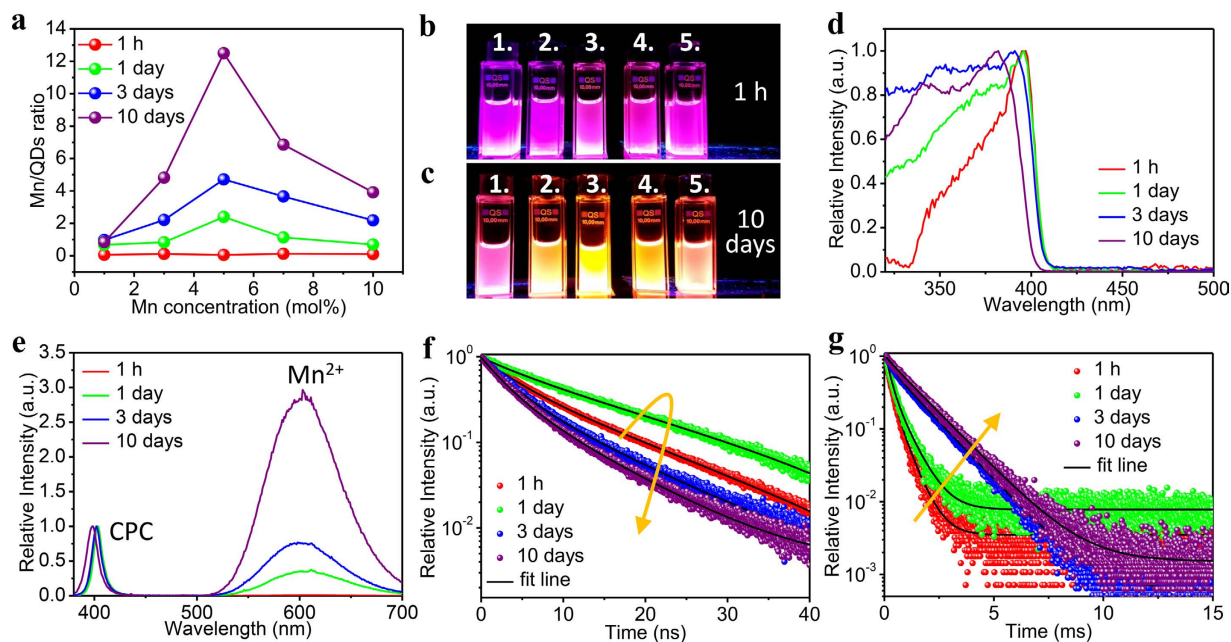


Figure 3. Spectral evolution of $\text{CsPbCl}_3:x\%\text{Mn}^{2+}$ ($x = 1, 3, 5, 7,$ and 10) QDs and $\text{CsPbCl}_3:5\%\text{Mn}^{2+}$ QDs as function of reaction time. (a) Mn^{2+} /Exciton emission ratio for different reaction times from 1 h to 10 days. Photographs of QD solutions under UV illumination after stirring for 1 h (b) and 10 days (c). Numbers (1 → 5) represent different Mn^{2+} concentration (1 → 10 mol%). (d) Excitation spectra and (e) emission spectra of $\text{CsPbCl}_3:5\%\text{Mn}^{2+}$ QDs with $10\ \mu\text{l}$ SiCl_4 . PL decays of CsPbCl_3 QD exciton emission (~ 400 nm) (f) and Mn^{2+} emission (~ 600 nm) (g) after 376.8 nm and 355 nm pulsed excitation.

is observed between 1 h and 10 days. As a result of increased Mn-incorporation the emission color shifts from violet to orange. Interestingly, the Mn/QD intensity ratios drastically increase after stirring for 1 day (green line). At all times, the highest Mn/QD ratio is found for a 5% Mn concentration. For higher nominal Mn-concentrations a drop in emission intensity is observed, possibly caused by concentration quenching. Concentration quenching is caused by energy transfer between dopant ions leading to migration to defects and quenching sites. Typically, this occurs at concentrations higher than 5% but as the distribution of the Mn^{2+} ions may not be homogeneous, a higher concentration of Mn^{2+} ions in the surface layer can explain a reduced luminescence intensity by concentration quenching through energy migration in a Mn-enriched surface layer. Based on this, it is concluded that the reaction conditions leading to CPC–Mn QDs with the highest Mn-emission intensity is CPC:5%Mn with $10\ \mu\text{l}$ SiCl_4 for the reaction volume (2 ml) and QD concentrations (20 mg/ml) used here. The changes in luminescence properties over time were followed for the CPC:5%Mn– SiCl_4 ($10\ \mu\text{l}$) by recording excitation and emission spectra as well as luminescence decay curves of the exciton and Mn^{2+} emission for samples taken after 1 h, and 1, 3, 10 days. The results are shown in Fig. 3d–g.

Focusing on the CPC:5%Mn– SiCl_4 ($10\ \mu\text{l}$) system, the results show a continued increase in the Mn^{2+} emission intensity relative to the excitonic emission (Fig. 3e) for reaction times up to 10 days. The excitation spectra of the Mn^{2+} emission show the characteristics of the CsPbCl_3 QD absorption spectrum, giving evidence for energy transfer from the QD exciton state to the Mn^{2+} dopant. For longer reaction times a blue shift in the first excitonic peak is observed, both in emission and excitation (Fig. 3d–e). The shift to shorter wavelengths can be explained by a decrease in the size of the QDs as a result of slow etching accompanying the Mn-incorporation process. As shown in Fig. 1 the QD size decreases from 12 to 8 nm after 10 days of stirring and this can explain the observed blue shift. The highest Mn^{2+} emission intensity is observed after 10 days of stirring. At longer times the intensity starts to decrease but even after 40 days a clear Mn^{2+} emission is observed with $\sim 30\%$ of the maximum emission intensity.

To gain further insight in the energy transfer process and incorporation of Mn^{2+} in the CPC QDs, luminescence decay curves were recorded for both the exciton and Mn^{2+} emission. Table 1 summarizes the lifetime (for QD exciton and Mn^{2+} emission) of CPC:5%Mn– SiCl_4 ($10\ \mu\text{l}$) for various reaction times. Energy transfer from the excitonic state to Mn^{2+} results in a faster exciton emission decay. The Mn^{2+} emission decay can be different for surface absorbed Mn^{2+} than for Mn^{2+} incorporated in the QD as energy transfer to defects or surface quenching sites is more prominent for surface Mn^{2+} resulting in shorter decay times for emission from surface Mn^{2+} ions. The luminescence decay dynamics were recorded for samples taken at several times during the incorporation of Mn^{2+} for the CPC:5%Mn– SiCl_4 ($10\ \mu\text{l}$) system as this was shown to give the most efficient Mn^{2+} emission. In Fig. 3f, the PL decay curves of the excitonic QD emission are shown. Initially, *i.e.* for the decay curves recorded for samples taken after 1 h to 1 day, a lengthening of the decay time is observed. The decay curve for the exciton emission from the sample stirred for 1 day is close to single exponential with a ~ 16 ns decay time. The initial lengthening of the decay time can be explained by improved surface passivation as a result of the chloride formation

Reaction times	Lifetime of QDs (ns)			Lifetime of Mn ²⁺ (ms)		
	τ_1	τ_2	τ_{avg}	τ_1	τ_2	τ_{avg}
no SiCl ₄	2.9	9.6	7.5	—	—	—
1 h	3.9	12.1	10.3	0.5	0.2	0.4
1 day	5.1	16.8	15.6	0.2	0.7	0.5
3 days	3.3	9.4	7.5	0.3	1.4	1.3
10 days	2.8	8.1	6.3	0.3	1.4	1.4

Table 1. Lifetimes of QD exciton and Mn²⁺ emission of the CPC:5%Mn–SiCl₄ (10 μ l) for various reaction times based on a bi-exponential fit of the luminescence decay curves.

following SiCl₄ decomposition. Better surface passivation by the Cl[−] ions remove surface trap states resulting in a more efficient excitonic emission. The 16 ns decay time can be considered to be close to the pure radiative decay time of the exciton emission at room temperature. The results agree with the observation of higher absolute (excitonic) emission intensities of CPC QDs in the initial reaction period (up to 1 day) as shown in Fig. S8a.

After prolonged reaction times, the Mn²⁺ emission intensity strongly increases, while the excitonic emission intensity decreases. Concurrently, the exciton emission decay becomes shorter and also non-exponential (blue and violet curves in Fig. 3f). After stirring for 10 days a τ_{avg} = 6.3 ns decay time is observed. The shortening of the decay time is explained by energy transfer from the QD exciton state to the Mn²⁺ dopants. The non-exponential character reflects that transfer rates vary for differently doped QDs. Undoped QDs still decay with the radiative exciton decay time while QDs with one or more Mn²⁺ ions will decay with a decay rate that is the sum of the radiative decay rate and the transfer rate. The exciton-to-Mn²⁺ transfer rate will also depend on the location of the Mn²⁺ ion in the CPC–Mn QD. Transfer to a centrally located Mn²⁺ ion is expected to be faster than to a Mn²⁺ ion in the outer shell of the QD where the overlap with excitonic wavefunction is smaller.

Figure 3g show the luminescence decay curves of the Mn²⁺ emission as a function of reaction time. Long decay times in the ms time regime are observed which is typical for the spin- and parity forbidden Mn²⁺ emission^{23,24}. Initially the decay curves are non-exponential and the faster initial decay reflects emission from Mn²⁺ at the QD surface where partial quenching by surface defect states introduces a fast non-radiative decay channel. For long reaction times (3 and 10 days) the decay is close to single exponential with a long 1.4 ms decay time suggesting that Mn²⁺ is incorporated inside the CPC host and decays with a ms radiative decay rate typical for the spin- and parity forbidden Mn²⁺ emission.

Reaction mechanism. The synthesis procedure and characterization discussed above provide strong evidence that addition of SiCl₄ to the CPC QDs in toluene in the presence of the Mn–stearate precursor results in the slow incorporation of Mn²⁺ in the CsPbCl₃ QDs. It is interesting to discuss potential incorporation mechanisms and the location of the Mn²⁺ ions in the CPC QDs. Control experiments help to provide insight in the mechanism. No incorporation of Mn²⁺ was observed after thorough washing of the CPC–Mn QDs with acetone before the addition of SiCl₄ (Fig. S7). This shows that the (apolar) Mn–precursor is adsorbed at the CPC QD surface after the initial QD synthesis procedure in the presence of the Mn–stearate precursor. A second control experiment involves dripping of SiCl₄ to the CPC QDs with Mn–precursor in toluene in vacuum. Again, no Mn–incorporation is observed under these conditions. Only the weak emission of Mn²⁺ ions around 590 nm and a faint blue emission, possibly from organic chromophores formed during ligand decomposition, were observed (Fig. S9). The absence of water prevents decomposition of SiCl₄ and demonstrates that hydrolysis of SiCl₄ is crucial in the reaction:



Hydrolysis of SiCl₄ gives rise to the formation of HCl that can react with the Mn–stearate precursor (releasing Mn²⁺) and with the CPC QD surface to both etch the surface (H⁺) and reconstruct the QD surface (Cl[−]). The blue shift of the excitonic emission with reaction time and the TEM images showing a decrease in particle size are consistent with the occurrence of etching of the CPC QDs. The SiO₂ formed during the decomposition reaction of SiCl₄ and H₂O gives rise to SiO₂ spheres observed in TEM and possibly also form a thin protective SiO₂ layer around the CPC QDs after prolonged reaction times. The increase of the QD exciton emission and lengthening of the exciton emission decay time in the initial hours after addition of SiCl₄ signifies the positive role of the HCl in the passivation of surface defect states. Similar observations were made previously for hybrid perovskite thin films³⁸. A remarkable increase in photoluminescence intensity and lengthening of the emission decay time was observed upon addition of phosphoric acid and explained by the removal of (surface) defect states³⁸. In addition to surface reconstruction, in the presence of Mn²⁺ and Cl[−] a Mn–Cl surface layer can form on the CPC QD. Etching and reconstruction of the CsPbCl₃ surface can occur with the incorporation of Mn²⁺ on Pb²⁺ sites in the surface layer of the CPC QDs. Subsequent diffusion of the Mn²⁺ into the CPC QD brings Mn²⁺ inside the CPC QDs, similar to the Mn²⁺ doping of CdSe QDs through diffusion doping²⁷. Fig. 4 illustrates the proposed reaction mechanism for the incorporation of Mn²⁺ and SiO₂ formation. The reaction mechanism is consistent with the long reaction times of hours to days observed for diffusion doping and cation exchange reactions at room temperature^{18,39}.

Further research is required to provide a more complete understanding of details on the incorporation mechanism. Based on the present experiments it cannot be excluded that the Mn²⁺ ions remain located in a surface layer of the CPC QDs. The observation of a transition from non-exponential decay to a single exponential 1.4 ms decay

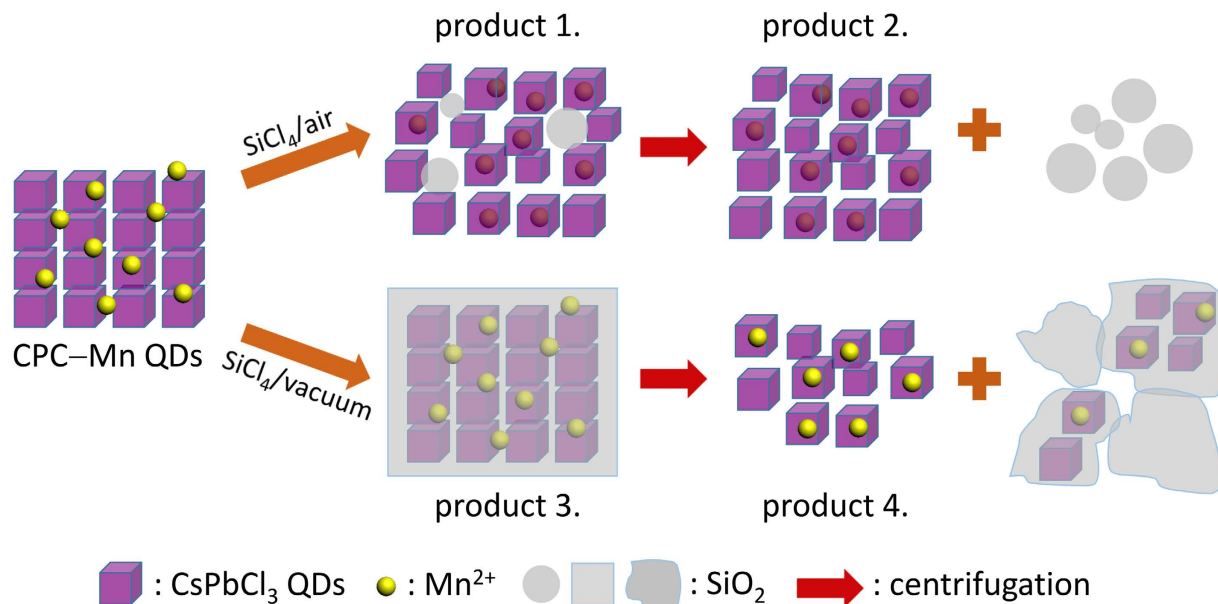


Figure 4. Schematic illustration of Mn²⁺ ions diffusion doping mechanism and SiO₂ formation. Purple cubes represent the CsPbCl₃ QDs; the yellow spheres represent the Mn²⁺ ions; the gray particles represent SiO₂; and the red arrows represent centrifugation.

of the Mn²⁺ emission is important as it gives evidence that the local surroundings for the Mn²⁺ ions changes during the reaction. Initially surface Mn²⁺ ions are present with a shorter life time because of the proximity of surface defect states. For longer reaction times the transition to a purely exponential decay indicates the transition to the same (octahedral) coordination by Cl⁻ for all Mn²⁺ ions. This observation however does not prove that the Mn²⁺ ions are homogeneously distributed through the CsPbCl₃ QD. The continued observation of exciton emission indicates that the transfer efficiency is limited and that the Mn²⁺ ions may be preferentially situated in the surface layer where the coupling with the excitonic wavefunction is weaker. Further research on incorporation of Mn²⁺ in other perovskite QDs is also interesting. For example, for CsPbBr₃ QDs the exciton shifts to lower energies (compared to CsPbCl₃) while, because of a smaller crystal field splitting for the weaker Br⁻ ligands, the Mn²⁺ emission is expected to shift to higher energies. This may lead to a cross-over between the exciton and Mn²⁺ emission depending on the quantum dot size, similar to what has been observed for Mn²⁺-doped CdSe quantum dots.²⁴

Stability. For practical application of perovskite quantum dots stability is an important issue. Thermal and photo stability are often limited for the Pb-halide perovskites and also sensitivity to moisture is serious issue that hampers the introduction of this new class of materials in products for the solar cell and lighting market^{40–42}. To evaluate the stability of the emission of the SiCl₄-modified CPC-Mn QDs solutions was followed over time. The emission intensity shows a slow decrease in intensity but retains 27% of the maximum intensity after 40 days in air, as shown in Fig. 5a. The temperature dependence of the photoluminescence was measured for CPC-Mn QDs (exciton emission) and SiCl₄-modified CPC-Mn QDs (Mn²⁺ emission) after incorporation in a poly methyl methacrylate (PMMA) matrix. The decrease of emission intensity with temperature is shown in Fig. 5b. At 100 °C the emission of CPC-Mn QDs is completely quenched, whereas the SiCl₄-modified CPC-Mn QDs maintained ~50% of their initial intensity.

In conclusion, we have reported a new doping strategy for the successful incorporation of Mn²⁺ ions in perovskite CsPbCl₃ QDs. Upon addition of SiCl₄ to a CsPbCl₃ QD/Mn-precursor dispersion in toluene incorporation of Mn²⁺ occurs as demonstrated by the evolution of strong 600 nm Mn²⁺ emission (⁴T₁ → ⁶A₁) following excitation in the QD exciton states. Excitation, emission and luminescence life time measurements reveal the presence of energy transfer from the delocalized QD exciton state to the localized 3d⁵ states of Mn²⁺. The proposed incorporation mechanism involves surface etching and reconstruction by HCl formed through decomposition of SiCl₄ in the presence of trace amounts of water in toluene. The presently reported synthesis approach is promising for exploring other transition-metal or lanthanide ion doped perovskite QDs in order to gain a wider control over the optical and magnetic properties of doped QDs for applications in the fields of lighting and spintronics.

Methods

Preparation of Cs-oleate. The synthesis approach has been reported by Kovalenko *et al.*¹³. In brief, Cs₂CO₃ (0.2035 g, Sigma Aldrich, 99.9%), oleic acid (0.625 ml, OA, Sigma Aldrich, 90%), and 1-octadecene (10 ml, ODE, Sigma Aldrich, 90%) were loaded into a 50 ml 3-neck flask and degassed under vacuum at 120 °C for 1 h. Subsequently, the solution was heated to 150 °C under N₂ for all Cs₂CO₃ reacting with OA.

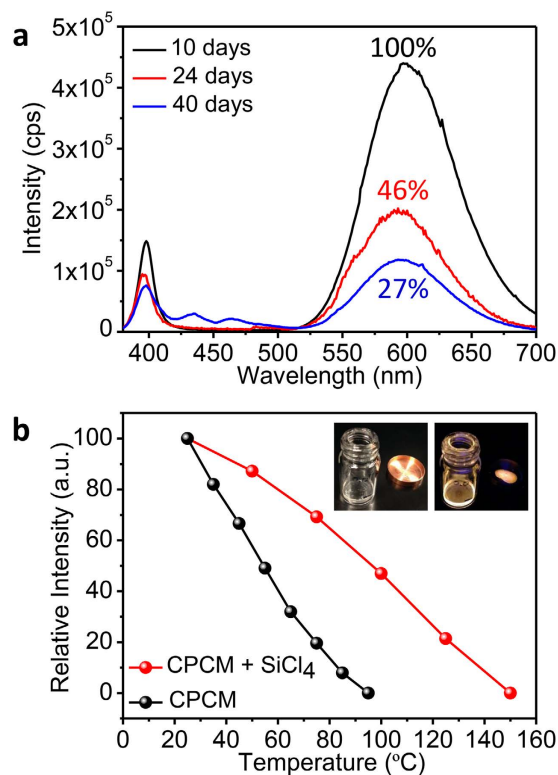


Figure 5. Stability of the $\text{CsPbCl}_3:5\%\text{Mn}^{2+}\text{-SiCl}_4$ (10 μl) system. (a) Emission spectra recorded after different stirring times in air. (b) Relative emission intensity as a function of the temperature for the Mn^{2+} emission in CPC-Mn-SiCl₄ (red line) and the exciton emission for the CPC QDs without SiCl₄ added. [Inset: photographs of the CPC:5%Mn-SiCl₄ QDs in ambient light (left) and under irradiation with a UV lamp (right). The CPC:5%Mn-SiCl₄ QDs are shown in a vial with PMMA and the resulting PMMA-QD polymer film on the copper heating block.] All measurements are done under 365 nm excitation.

Preparation of $\text{CsPb}_{1-x}\text{Cl}_3:x\%\text{Mn}^{2+}$ NCs. PbCl₂ (0.0497 g, Sigma Aldrich, 99.999%), C₃₆H₇₀MnO₄ (x = 5; 0.0058 g, Chemos GmbH), and ODE (5 ml) were loaded into a 25 ml 3-neck flask and degassed under vacuum at 120 °C for 1 h. Afterwards, dried oleylamine (0.5 ml, OLA, Sigma Aldrich, 70%) and OA (0.5 ml) were injected into the solution at 120 °C under N₂ atmosphere. The temperature was raised to 170 °C and Cs-oleate solution (0.4 ml) was quickly injected into the mixture. After the desired different reaction time, the mixture was cooled by the ice-water bath. The NCs were extracted from the crude solution through centrifuging at 3500 r.p.m. for 10 min. First, the supernatant was discarded and the precipitated particles were redispersed in toluene forming the stable colloidal solution. Second, the colloidal solution was centrifuged again, and the precipitated particles were discarded and the supernatant was redispersed in toluene forming the final solution.

Addition of silicon tetrachloride (SiCl₄). Various amounts of SiCl₄ (Sigma Aldrich, 99%) were introduced into a 20 ml sample bottle containing 2 ml of the colloidal CPC-Mn QDs toluene solution (H₂O content 0.0623%)³¹. After different stirring time, the white precipitates (SiO₂) and the transparent solutions were separated through centrifuging at 10000 r.p.m. for 10 min. In a control experiment, 10 μl SiCl₄ was mixed with CPC-Mn QDs (nearly water free) in a vacuum three-necked flask.

Preparation of $\text{CsPbCl}_3:\text{Mn}^{2+}$ bulk material. The CPC-Mn microcrystalline powder was prepared by melting starting material in an evacuated and sealed quartz ampoule⁴³. High-purity CsCl (Brunswick Chemie B.V., 99.9%), PbCl₂ (Sigma Aldrich, 99.999%), and MnCl₂ (Sigma Aldrich, 99%) were mixed thoroughly and loaded into a quartz ampoule. The ampoule was evacuated and suspended with platinum wire in the high temperature region of a sintering furnace. The temperature was raised to 300 °C with a heating rate of 5 °C/min and kept for 2 h under continuous pumping to remove surface absorbed water. Then, the ampoule was sealed and the sample was sintered at 675 °C for 1 h, after which the sample was allowed to naturally cool to room temperature in the furnace.

Polymerization reaction of CPC:5%Mn-SiCl₄ + PMMA. PMMA (0.8 g) powder was dispersed homogeneously in toluene (2 ml) for stirring 1 day. Then CPC:5%Mn-SiCl₄ QDs (20 mg) were added into the PMMA-toluene solution and stirred for 1 day. The transparent mixture was dripped into a glass container and a copper hold, as shown in the inset of Fig. 5b. The polymerization took place under a vacuuming procedure for 1 day.

X-ray diffraction. XRD patterns were recorded using Cu K α radiation ($\lambda = 1.5418 \text{ \AA}$) on a PW 1729 Philips diffractometer, operating at 40 kV and 20 mA. For XRD analysis, the samples were prepared by depositing the QDs colloidal solution on the silicon wafer and evaporating the solvent under vacuum atmosphere.

Optical Characterization. Absorption spectra were obtained using a Perkin–Elmer Lambda 950 UV/VIS/IR spectrophotometer. Excitation and emission spectra were measured by an Edinburgh Instruments FLS920 spectrofluorometer equipped with a 450 W Xenon lamp. Visible emission (400–850 nm) was detected by a Hamamatsu R928 photomultiplier tube (PMT).

Lifetime. Photoluminescence (PL) decay curves of the CsPbCl₃ QDs were recorded by using an Edinburgh Instruments diode laser with an excitation wavelength of 376.8 nm (65 ps pulse width, 0.2–20 MHz repetition rate) and a Hamamatsu H74220–02 PMT in combination with the Edinburgh spectrofluorometer. PL decay measurements of the Mn²⁺ dopants were done using an optical parametric oscillator (OPO) system (Opotek HE 355 II) pumped by the third harmonic of a Nd:YAG laser as excitation source and a Hamamatsu R928 PMT as light detection. The samples for optical analysis were prepared by dissolving the crude QDs production in toluene in a quartz cuvette.

Electron Microcopy and Energy Dispersive X-ray Spectroscopy. Scanning transmission electron microscopy (STEM) images and Energy dispersive X-ray spectroscopy (EDX) measurements were performed using a TalosTM F200X transmission electron microscope (from FEI), equipped with a high-brightness field emission gun (X-FEG) and a Super-X G2 EDX detector operated at 200 kV. TEM images were obtained using FEI TECNAI T12, operating at 120 kV. The samples for TEM imaging were prepared by depositing the QDs colloidal solution on the carbon-coated copper TEM grid and evaporating the solvent under inert atmosphere.

References

- Xing, G. *et al.* Long-range balanced electron- and hole-transport lengths in organic–inorganic CH₃NH₃PbI₃. *Science* **342**, 344–347 (2013).
- Stranks, S. D. *et al.* Electron–hole diffusion lengths exceeding 1 micrometer in an organometal trihalide perovskite absorber. *Science* **342**, 341–344 (2013).
- Gratzel, M. The light and shade of perovskite solar cells. *Nat. Mater.* **13**, 838–842 (2014).
- Dohner, E. R., Jaffe, A., Bradshaw, L. R. & Karunadasa, H. I. Intrinsic white-light emission from layered hybrid perovskites. *J. Am. Chem. Soc.* **136**, 13154–13157 (2014).
- Li, G. *et al.* Efficient light-emitting diodes based on nanocrystalline perovskite in a dielectric polymer matrix. *Nano Lett.* **15**, 2640–2644 (2015).
- Sutherland, B. R., Hoogland, S., Adachi, M. M., Wong, C. T. O. & Sargent, E. H. Conformal organohalide perovskites enable lasing on spherical resonators. *ACS Nano* **8**, 10947–10952 (2014).
- Zhu, H. *et al.* Lead halide perovskite nanowire lasers with low lasing thresholds and high quality factors. *Nat. Mater.* **14**, 636–642 (2015).
- Dou, L. *et al.* Solution-processed hybrid perovskite photodetectors with high detectivity. *Nat. Commun.* **5**, 5404 (2014).
- Maculan, G. *et al.* CH₃NH₃PbCl₃ single crystals: inverse temperature crystallization and visible–blind UV–photodetector. *J. Phys. Chem. Lett.* **6**, 3781–3786 (2015).
- Park, N. G. Organometal perovskite light absorbers toward a 20% efficiency low-cost solid-state mesoscopic solar cell. *J. Phys. Chem. Lett.* **4**, 2423–2429 (2013).
- Zhou, H. *et al.* Interface engineering of highly efficient perovskite solar cells. *Science* **345**, 542–546 (2014).
- Yang, Z. *et al.* Colloidal quantum dot photovoltaics enhanced by perovskite shelling. *Nano Lett.* **15**, 7539–7543 (2015).
- Protesescu, L. *et al.* Nanocrystals of cesium lead halide perovskites (CsPbX₃, X = Cl, Br, and I): novel optoelectronic materials showing bright emission with wide color gamut. *Nano Lett.* **15**, 3692–3696 (2015).
- Nedelcu, G. *et al.* Fast anion-exchange in highly luminescent nanocrystals of cesium lead halide perovskites (CsPbX₃, X = Cl, Br, I). *Nano Lett.* **15**, 5635–5640 (2015).
- Swarnkar, A. *et al.* Colloidal CsPbBr₃ perovskite nanocrystals: luminescence beyond traditional quantum dots. *Angew. Chem. Int. Ed.* **54**, 15424–15428 (2015).
- Nikl, M. *et al.* Quantum size effect in the excitonic luminescence of CsPbX₃-like quantum dots in CsX (X = Cl, Br) single crystal host. *J. Lumin.* **72–4**, 377–379 (1997).
- Beaulac, R., Ochsenein, S. T. & Gamelin, D. R. Colloidal transition–metal–doped quantum dots. In *nanocrystal quantum dots*; Klimov, V. I., ed.; CRC Press: New York, 397–453 (2010).
- Beaulac, R., Archer, P. I., Ochsenein, S. T. & Gamelin, D. R. Mn²⁺-doped CdSe quantum dots: new inorganic materials for spin-electronics and spin-photonics. *Adv. Funct. Mater.* **18**, 3873–3891 (2008).
- Bhattacharyya, S., Zitoun, D. & Gedanken, A. Electron paramagnetic resonance spectroscopic investigation of manganese doping in ZnL (L = O, S, Se, Te) nanocrystals. *Nanosci. Nanotechnol. Lett.* **3**, 541–549 (2011).
- Stefan, M., Nistor, S. V. & Ghica, D. ZnS and ZnO semiconductor nanoparticles doped with Mn²⁺ ions. Size effects investigated by EPR spectroscopy. In size effects in nanostructures. Kuncser, V., Miu, L., eds; *Springer Series in Materials Science*, Vol. 205, Part 1; Springer: Berlin, Heidelberg, 3–27 (2014).
- Baranov, P. G., Orlinskii, S. B., De Mello Donega, C. & Schmidt, J. High-frequency EPR, ESE, and ENDOR spectroscopy of Co- and Mn-doped ZnO quantum dots. *Phys. Status Solidi B* **250**, 2137–2140 (2013).
- Jana, S., Manna, G., Srivastava, B. B. & Pradhan, N. Tuning the emission colors of semiconductor nanocrystals beyond their bandgap tunability: all in the dope. *Small* **9**, 3753–3758 (2013).
- Erwin, S. C. *et al.* Doping semiconductor nanocrystals. *Nature* **436**, 91–94 (2005).
- Beaulac, R., Archer, P. I., van Rijssel, J., Meijerink, A. & Gamelin, D. R. Exciton storage by Mn²⁺ in colloidal Mn²⁺-doped CdSe quantum dots. *Nano Lett.* **8**, 2949–2953 (2008).
- Erickson, C. S. *et al.* Zero-reabsorption doped–nanocrystal luminescent solar concentrators. *ACS Nano* **8**, 3461–3467 (2014).
- Suyver, J. F., Wuister, S. F., Kelly, J. J. & Meijerink, A. Synthesis and photoluminescence of nanocrystalline ZnS:Mn²⁺. *Nano Lett.* **1**, 429–433 (2001).
- Vlaskin, Vladimir A., Barrows, Charles J., Erickson, Christian S. & Gamelin, D. R. Nanocrystal diffusion doping. *J. Am. Chem. Soc.* **135**, 14380–14389 (2013).
- Parobek, D. *et al.* Exciton-to-dopant energy transfer in Mn-doped cesium lead halide perovskite nanocrystals. *Nano Lett.* **16**, 7376–7380 (2016).

29. Liu, W. Y. *et al.* Mn²⁺-doped lead halide perovskite nanocrystals with dual-color emission controlled by halide content. *J. Am. Chem. Soc.* **138**, 14954–14961 (2016).
30. Kim, Y. *et al.* Efficient luminescence from perovskite quantum dot solids. *ACS Appl. Mater. Interfaces* **7**, 25007–25013 (2015).
31. Huang, S. *et al.* Enhancing the stability of CH₃NH₃PbBr₃ quantum dots by embedding in silica spheres derived from tetramethyl orthosilicate in “waterless” toluene. *J. Am. Chem. Soc.* **138**, 5749–5752 (2016).
32. Zhang, T. *et al.* Cellular effect of high doses of silica-coated quantum dot profiled with high throughput gene expression analysis and high content cellomics measurements. *Nano Lett.* **6**, 800–808 (2006).
33. Jun, S., Lee, J. & Jang, E. Highly luminescent and photostable quantum dot-silica monolith and its application to light-emitting diodes. *ACS Nano* **7**, 1472–1477 (2013).
34. Fardad, M. A. Catalysts and the structure of SiO₂ sol-gel films. *J. Mater. Sci.* **35**, 1835–1841 (2000).
35. Ibrahim, I. A. M., Zikry, A. A. F. & Sharaf, M. A. Preparation of spherical silica nanoparticles: Stober silica. *J. Am. Sci.* **6**, 985–989 (2010).
36. Ramírez-Serrano, J., Madrigal, E., Ramos, F. & Caldiño Garcia, U. Optical spectroscopy of Mn²⁺ ions in CdCl₂ single crystals. *J. Lumin.* **71**, 169–175 (1997).
37. Marco de Lucas, M. C., Rodri'guez, F., Gu'ndel, H. U. & Furer, N. Optical properties of the MnCl₄[−] complex formed in ABCl₃:Mn²⁺ pseudoperovskite crystals: Influence of the chemical pressure. *J. Lumin.* **60**, 581–584 (1994).
38. Zhang, W. *et al.* Enhanced optoelectronic quality of perovskite thin films with hypophosphorous acid for planar heterojunction solar cells. *Nat. Commun.* **6**, 10030 (2015).
39. Trizio, L. D. & Manna, L. Forging colloidal nanostructures via cation exchange reactions. *Chem. Rev.* **116**, 10852–10887 (2016).
40. Noh, J. H., Im, S. H., Heo, J. H., Mandal, T. N. & Seok, S. I. Chemical management for colorful, efficient, and stable inorganic-organic hybrid nanostructured solar cells. *Nano Lett.* **13**, 1764–1769 (2013).
41. Smith, I. C., Hoke, E. T., Solis-Ibarra, D., McGehee, M. D. & Karunadasa, H. I. A layered hybrid perovskite solar-cell absorber with enhanced moisture stability. *Angew. Chem. Int. Ed.* **53**, 1–5 (2014).
42. Luo, B. *et al.* Organolead halide perovskite nanocrystals: branched capping ligands control crystal size and stability. *Angew. Chem. Int. Ed.* **55**, 8864–8868 (2016).
43. Midorikawa, M., Ishibashi, Y. & Takagi, Y. Optical and dilatometric studies of KCaCl₃ and RbCaCl₃ Crystals. *J. Phys. Soc. Japan* **46**, 1240–1244 (1979).

Acknowledgements

This work was supported by the Ministry of Science and Technology of Taiwan (Contract No. MOST 104–2917–I–564–060). We thank Prof. Alfons van Blaaderen for provide beneficial suggestions. We thank Chenghui Xia for help to measure some PL data. Da Wang acknowledges partial funding from the European Research Council under the European Union's Seventh Framework Programme (FP–2007–2013)/ERC Advanced Grant Agreement 291667 HierarSACol.

Author Contributions

C.C.L. conceived the idea of the synthesis method and performed the synthesis, measurement and characterization. K.Y.X. synthesized the CPC–Mn powder and analysis. D.W. contributed to TEM measurement and analysis. A.M. revised the manuscript and supervised the project. C.C.L. wrote the first version of the manuscript and all authors discussed the results and contributed to the final version of the paper.

Additional Information

Supplementary information accompanies this paper at <http://www.nature.com/srep>

Competing Interests: The authors declare no competing financial interests.

How to cite this article: Lin, C.C. *et al.* Luminescent manganese-doped CsPbCl₃ perovskite quantum dots. *Sci. Rep.* **7**, 45906; doi: 10.1038/srep45906 (2017).

Publisher's note: Springer Nature remains neutral with regard to jurisdictional claims in published maps and institutional affiliations.



This work is licensed under a Creative Commons Attribution 4.0 International License. The images or other third party material in this article are included in the article's Creative Commons license, unless indicated otherwise in the credit line; if the material is not included under the Creative Commons license, users will need to obtain permission from the license holder to reproduce the material. To view a copy of this license, visit <http://creativecommons.org/licenses/by/4.0/>

© The Author(s) 2017